Received July 22, 2017, accepted August 14, 2017, date of publication August 23, 2017, date of current version September 19, 2017.

Digital Object Identifier 10.1109/ACCESS.2017.2743213

UWB-Based Indoor Human Localization With Time-Delayed Data Using EFIR Filtering

YUAN XU[1], (Member, IEEE), YURIY S. SHMALIY[2], (Fellow, IEEE), YUEYANG LI[1], (Member, IEEE), AND XIYUAN CHEN[3], (Senior Member, IEEE)

[1]School of Electrical Engineering, University of Jinan, Jinan 250022, China
[2]Department of Electronics Engineering, Universidad de Guanajuato, Salamanca 36885, Mexico
[3] School of Instrument Science and Engineering, Southeast University, Nanjing 210096, China

Corresponding authors: Yuan Xu (xy_abric@126.com) and Yueyang Li (cse_liyy@ujn.edu.cn)

This work was supported in part by the National Natural Science Foundation of China under Grant 61203083 and Grant 51375087, in part by the Shandong Provincial Natural Science Foundation, China, under Grant ZR2017QF007, and in part by the Doctoral Foundation of the University of Jinan under Grant XBS1503 and Grant XBS1501.

ABSTRACT An ultra wide band (UWB)-based time-delay indoor human localization scheme is proposed to provide indoor human localization with time-delay measurements. The human position is localized using the UWB-based distance data and the extended finite impulse response (EFIR) estimator employing the time-delay localization model. Only one-step delayed measurements are considered in this paper. We employ the state augmentation method to combine the delayed and not delayed states. To improve the localization robustness for the time-delay localization model, we employ the EFIR filter, which does not require the noise statistics. The experimental results have shown that the EFIR estimator is more robust than the extended Kalman filter-based one for the delayed data.

INDEX TERMS Indoor localization, ultra wide band, extended FIR filter, extended Kalman filter, time-delay model.

I. INTRODUCTION

Nowadays, indoor human localization has become one of the most important topics [1]–[3]. In the localization technology, the Global Positioning System (GPS) is one of the most widely used [4]. But even though the GPS can provide the human position information universally, its signals may not always be available in indoor environments [5]. In order to provide accurate position information in indoor environments, some local positioning system (LPS)-based technologies have been proposed. For example, in [6]–[8], the WiFi has been used to provided the localization in complex indoor environment; the radio frequency identification (RFID) tag environments were exploited in [9]–[11] to provide object self-localization. Although the WiFi-based and the RFID-based LPS technologies are universal for human location in indoor environments, their localization accuracy stays at a meter level. To increase the resolution, the use of the ultra wide band (UWB) technology has been proposed by some researches. For example, in [12] and [13], the UWB is used to track the target in indoor environment and we notice that the use of UWB improves the accuracy from a meter level to a centimeter level.

The widely used models for single technology-based data fusion in human localization are the constant velocity (CV) model [14], the constant acceleration (CA) model [15], and the singer model [16], [17]. Although these methods allow for the estimation of the target location with a higher accuracy, they do not account for the delayed data, which can often be observed in practice [18]–[20]. It is especially true for the UWB-based localization system, where data derived from the sensor are transmitted wirelessly with possible delays. In order to overcome this problem, some estimators have been developed for time-delay data [21]–[24]. For example, in [25], the estimation for time-delay data is provided for robot manipulators; a distributed fusion estimation with missing measurements, random transmission delays, and packet dropouts is proposed in [26].

Data fusion is frequently used in accurate localization. Most often, the fusion filters are designed employing the Kalman filter (KF) algorithm in view of its optimality, simplicity, real-time operation, and small memory required [27]. Several efficient modifications of the KF were also proposed for nonlinear models. Among them the extended KF (EKF) [28], the unscented KF (UKF) [29], and the

2169-3536 © 2017 IEEE. Translations and content mining are permitted for academic research only.
Personal use is also permitted, but republication/redistribution requires IEEE permission.
See http://www.ieee.org/publications_standards/publications/rights/index.html for more information.

cubature KF (CKF) [30] have gained most currency. Let us notice that the performance of the KF-based filters critically depends on the noise statistics. If such information is unavailable, the KF estimate may severely degrade that can often be observed in practice. A better practical solution is the finite impulse response (FIR) structure, because it has been found that the limited memory filter has highest robustness [31], [32]. The most well developed iterative unbiased FIR (UFIR) filtering algorithm does not require the noise statistics, but its accuracy critically depends on the averaging horizon of N points, which must be optimal. For nonlinear models, the iterative extended UFIR (EFIR) filtering algorithm has been designed in [33].

In this paper, we propose an ultra wide band (UWB)-based time-delay indoor human localization scheme, in which the state augmentation method is used to combine the time-delayed and not delayed states. The EFIR estimator is used to fuse the distance data and provide the robust human position information. The EFIR-based time-delay model performance is compared to that of the EKF. The remaining part of this paper is organized as follows. Section II discusses the model for indoor UWB-based human localization with time-delayed data. Section III presents the EKF and EFIR algorithms. Experimental testing and discussions are given in Section IV. Finally, conclusions are drawn in Section V.

II. MODEL FOR INDOOR UWB-BASED HUMAN LOCALIZATION WITH TIME-DELAY MEASUREMENTS

A detailed structure of the human localization scheme using UWB-based measurements and discussed in this section is shown in Fig. 1. Here, the reference nodes (RNs) are mounted at fixed positions with known coordinates. The blind node (BN) measures the time of arrival (TOA) between the BN and the RNs and the distances are calculated via the TOA-distance model. Then, the distances are united as the measurement signal and sent to the EFIR filter, which is run by a computer to estimate the human position.

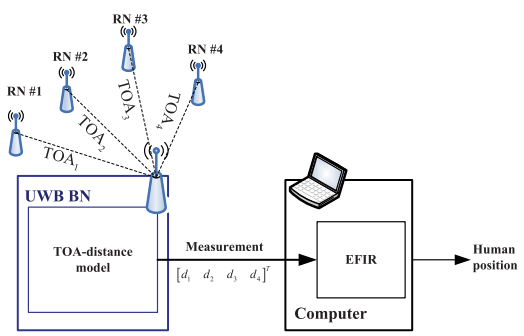

FIGURE 1. A detailed structure of the human localization system using UWB-based measurements.

A. STATE-SPACE MODEL WITH NO DELAY

If the transmission of measured data is provided with no delay, the human state equation can be written at time index k as

$$\underbrace{\begin{bmatrix} P_{E,k} \\ V_{E,k} \\ P_{N,k} \\ V_{N,k} \end{bmatrix}}_{\mathbf{x}^{ntd}_{k|k-1}} = \underbrace{\begin{bmatrix} 1 & T & 0 & 0 \\ 0 & 1 & 0 & 0 \\ 0 & 0 & 1 & T \\ 0 & 0 & 0 & 1 \end{bmatrix}}_{\mathbf{F}^{ntd}_{k-1}} \underbrace{\begin{bmatrix} P_{E,k-1} \\ V_{E,k-1} \\ P_{N,k-1} \\ V_{N,k-1} \end{bmatrix}}_{\mathbf{x}^{ntd}_{k-1}} + \mathbf{w}^{ntd}_{k-1} \quad (1)$$

where ntd means a model with no delay; T is the sampling time; $P_{E,k}$ and $P_{N,k}$ are the human position in the east and north directions, respectively; $V_{E,k}$ and $V_{N,k}$ are the human velocity in the east and north directions, respectively; and $\mathbf{w}^{ntd}_k$ is white Gaussian noise with zero mean and the covariance $\mathbf{Q}^{ntd}_k$.

With no data delays, the observation equation representing measurements with fused data (Fig. 1) can be written as

$$\underbrace{\begin{bmatrix} d_{1,k} \\ d_{2,k} \\ d_{3,k} \\ d_{4,k} \end{bmatrix}}_{\mathbf{y}^{ntd}_k} = \underbrace{\begin{bmatrix} \sqrt{\left(P_{E,k} - P^{(1)}_{E,k}\right)^2 + \left(P_{N,k} - P^{(1)}_{N,k}\right)^2} \\ \sqrt{\left(P_{E,k} - P^{(2)}_{E,k}\right)^2 + \left(P_{N,k} - P^{(2)}_{N,k}\right)^2} \\ \sqrt{\left(P_{E,k} - P^{(3)}_{E,k}\right)^2 + \left(P_{N,k} - P^{(3)}_{N,k}\right)^2} \\ \sqrt{\left(P_{E,k} - P^{(4)}_{E,k}\right)^2 + \left(P_{N,k} - P^{(4)}_{N,k}\right)^2} \end{bmatrix}}_{h(\mathbf{x}^{ntd}_k)} + \mathbf{v}^{ntd}_k \quad (2)$$

where $P^{(i)}_{E,k}$ and $P^{(i)}_{N,k} (i = 1, 2, 3, 4)$ are the RN positions in the east and north directions at time index k, respectively; $P_{E,k}$ and $P_{N,k}$ are the positions derived from UWB in the east and north directions, respectively; $d_{i,k} (i = 1, 2, 3, 4)$ is the distance between ith RN and BN; and $\mathbf{v}^{ntd}_k$ is white Gaussian noise with zero mean and the covariance $\mathbf{R}^{ntd}_k$.

B. STATE-SPACE MODEL WITH TIME-DELAYED DATA

In the UWB-based positioning system, time delays may be caused by the finite-time data transmission from the sensor to the receiver. For the time-delayed data, we employ the method of state augmentation to combine the delayed and not delayed states. In our particular situation, the measurement is observed with a delay on one time-step. Therefore, the state equation for the UWB-based human localization system can be written as

$$\underbrace{\begin{bmatrix} \mathbf{x}^{ntd}_k \\ \mathbf{x}^{ntd}_{k-1} \end{bmatrix}}_{\mathbf{x}^{td}_{k|k-1}} = \underbrace{\begin{bmatrix} \mathbf{F}^{ntd}_{k-1} & \mathbf{0} \\ \mathbf{I} & \mathbf{0} \end{bmatrix}}_{\mathbf{F}^{td}_{k-1}} \underbrace{\begin{bmatrix} \mathbf{x}^{ntd}_{k-1} \\ \mathbf{x}^{ntd}_{k-2} \end{bmatrix}}_{\mathbf{x}^{td}_{k-1}} + \mathbf{w}^{td}_{k-1}, \quad (3)$$

where td means "time-delay" and ntd "no delay"; the state vector $\mathbf{x}^{td}_k$ is composed by the state vectors $\mathbf{x}^{ntd}_k$ and $\mathbf{x}^{ntd}_{k-1}$; and $\mathbf{w}^{td}_k$ is white Gaussian noise with zero mean and the covariance $\mathbf{Q}^{td}_k$.

Algorithm 1 EKF Algorithm

Data: $\mathbf{y}_k^{td}, \mathbf{x}_0^{td}, \mathbf{P}_0^{td}, \mathbf{Q}_k^{td}, \mathbf{R}_k^{td}$
Result: $\hat{\mathbf{x}}_k^{td}$
begin
  for $k = 1 : SampleNumb$ **do**
    $\hat{\mathbf{x}}_{k|k-1}^{td} = \mathbf{F}_k^{td}\hat{\mathbf{x}}_{k-1}^{td}$
    $\mathbf{P}_{k|k-1}^{td} = \mathbf{F}_k^{td}\mathbf{P}_{k-1}^{td}(\mathbf{F}_k^{td})^T + \mathbf{Q}_k^{td}$
    $\mathbf{K}_k^{td} = \mathbf{P}_{k|k-1}^{td}(\mathbf{H}_k^{td})^T[\mathbf{H}_k^{td}\mathbf{P}_{k|k-1}^{td}(\mathbf{H}_k^{td})^T + \mathbf{R}_k^{td}]^{-1}$
    $\hat{\mathbf{x}}_k^{td} = \hat{\mathbf{x}}_{k|k-1}^{td} + \mathbf{K}_k^{td}[\mathbf{y}_k^{td} - h(\hat{\mathbf{x}}_{k|k-1}^{td})]$
    $\mathbf{P}_k^{td} = \left(\mathbf{I} - \mathbf{K}_k^{td}\mathbf{H}_k^{td}\right)\mathbf{P}_{k|k-1}^{td}$
  end for
end
† $\mathbf{H}_k^{td} = \left.\frac{\partial h(\mathbf{x}_k^{td})}{\partial \mathbf{x}_k^{td}}\right|_{\hat{x}_k^{td}}$

The observation equation of time-delay model can be written as

$$\underbrace{\begin{bmatrix} \mathrm{d}_{1,k-1} \\ \mathrm{d}_{2,k-1} \\ \mathrm{d}_{3,k-1} \\ \mathrm{d}_{4,k-1} \end{bmatrix}}_{\mathbf{y}_k^{td}} = \underbrace{\begin{bmatrix} \sqrt{\left(P_{E,k-1} - P_{E,k-1}^{(1)}\right)^2 + \left(P_{N,k-1} - P_{N,k-1}^{(1)}\right)^2} \\ \sqrt{\left(P_{E,k-1} - P_{E,k-1}^{(2)}\right)^2 + \left(P_{N,k-1} - P_{N,k-1}^{(2)}\right)^2} \\ \sqrt{\left(P_{E,k-1} - P_{E,k-1}^{(3)}\right)^2 + \left(P_{N,k-1} - P_{N,k-1}^{(3)}\right)^2} \\ \sqrt{\left(P_{E,k-1} - P_{E,k-1}^{(4)}\right)^2 + \left(P_{N,k-1} - P_{N,k-1}^{(4)}\right)^2} \end{bmatrix}}_{h(\mathbf{x}_k^{td})} + \mathbf{v}_k^{td} \tag{4}$$

where $\mathbf{v}_k^{td}$ is white Gaussian noise with zero mean and the covariance $\mathbf{R}_k^{td}$.

Given the state-space model (3) and (4), the EFIR can now be designed to provide accurate and robust estimation of the human coordinates as shown in Fig. 1.

III. ALGORITHMS FOR UWB-BASED HUMAN LOCALIZATION SYSTEM

In this section, applications of the EKF and robust EFIR algorithms will be discussed for the model (3) and (4).

A. EKF ALGORITHM

For the nonlinear observation equation (4), an application of the EKF algorithm has no essential specifics and its pseudo code can be listed as Algorithm 1. Note that the mapping matrix $\mathbf{H}_k^{td}$ is Jacobian and its computation must be provided at each time index k. Therefore, this matrix is always time-varying. An obvious disadvantage of the EKF algorithm is in the required noise covariances $\mathbf{Q}_k^{td}$ and $\mathbf{R}_k^{td}$, which may not be known exactly in practice especially for time-varying models. If so, the EKF may essentially lose in accuracy or precision to mean that it is not a robust estimator. Under the unknown or not well-known noise statistics, the EKF may diverge and its performance becomes worse in the presence of uncertainties and missing data.

Algorithm 2 EFIR Filtering Algorithm

1 **Data**: $\mathbf{y}_k^{td}, \mathbf{z}_k^{td}, M, N$
2 **Result**: $\hat{\mathbf{x}}_k^{td}$
3 **begin**
4 **for** $k = N - 1 : SampleNumb$ **do**
5 $m = k - N + 1, \quad s = m + M - 1$
6 $\tilde{\mathbf{x}}_s^{td} = \begin{cases} \mathbf{z}_s^{td}, & if\ s < N - 1 \\ \hat{\mathbf{x}}_s^{td}, & if\ s \geq N - 1 \end{cases}$
7 $\mathbf{G}_s^{td} = \mathbf{I}$
8 **for** $j = s + 1 : k$ **do**
9 $\tilde{\mathbf{x}}_{j|j-1}^{td} = \mathbf{F}_j^{td}\tilde{\mathbf{x}}_{j-1}^{td}$
10 $\mathbf{G}_j^{td} = \left[(\mathbf{H}_l^{td})^T\mathbf{H}_j^{td} + \left(\mathbf{F}_j^{td}\mathbf{G}_{j-1}^{td}(\mathbf{F}_j^{td})^T\right)^{-1}\right]^{-1}$
11 $\mathbf{K}_j^{td} = \mathbf{G}_j^{td}(\mathbf{H}_j^{td})^T$
12 $\tilde{\mathbf{x}}_j^{td} = \tilde{\mathbf{x}}_{j|j-1}^{td} + \mathbf{K}_j^{td}(\mathbf{y}_j^{td} - h(\tilde{\mathbf{x}}_{j|j-1}^{td}))$
13 **end for**
14 $\hat{\mathbf{x}}_k^{td} = \tilde{\mathbf{x}}_k^{td}$
15 **end for**
16 **end**
17 † M is the size of the error state vector
18 † N is the averaging horizon
19 † $\mathbf{z}_k^{td}$ is a vector of linear measurements of $\mathbf{x}_k^{td}$
20 † $\mathbf{H}_k^{td} = \left.\frac{\partial h(\mathbf{x}_k^{td})}{\partial \mathbf{x}_k^{td}}\right|_{\hat{\mathbf{x}}_k^{td}}$

B. ROBUST EFIR FILTERING ALGORITHM

A better solution can be the EFIR filter, which does not require any information about noise and is blind on given horizons [33]. To produce a suboptimal estimate, the averaging horizon for the EFIR filter must be set optimally. Following [32] and based on the state-space model (3) and (4), a pseudo code of the iterative EFIR filtering algorithm is listed Algorithm 2. As can be seen, Algorithm 2 has two main blocks. The first one computes the initial estimate $\tilde{\mathbf{x}}_s^{td}$ and generalized noise power gain (GNPG) $\mathbf{G}_s^{td}$ (lines 4–5), where M is the size of the state vector. The second block updates these values iteratively (lines 6–11) by changing an auxiliary variable j from $s + 1$ to k. The output estimate is taken when j reaches k (line 12). The bias correction gain for the iterative EFIR algorithm is computed as

$$\mathbf{K}_j^{td} = \mathbf{G}_j^{td}(\mathbf{H}_j^{td})^T \tag{5}$$

and we notice that it is not the Kalman gain.

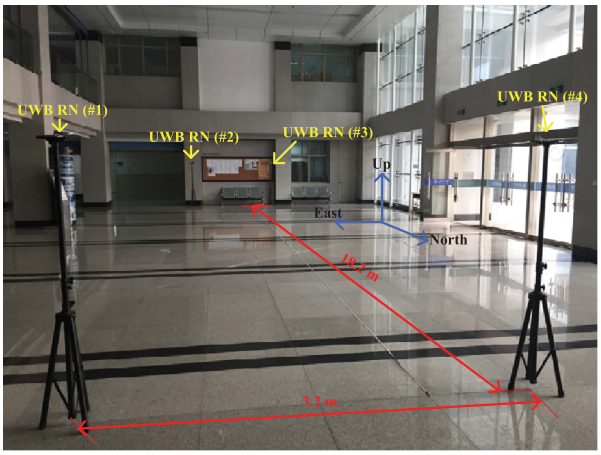

FIGURE 2. The indoor floorspace experimental environment created to test the human localization system shown in Fig. 1.

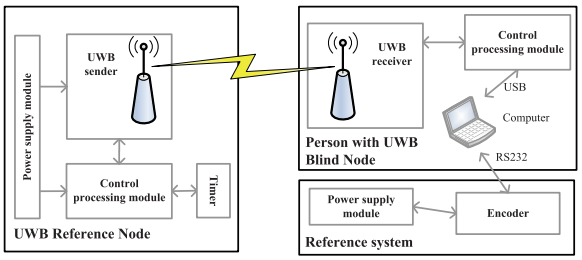

FIGURE 3. Architecture of the experimentally organized testbed for the proposed human localization system.

FIGURE 4. The human equipment used to test the proposed localization system.

IV. EXPERIMENTAL VERIFICATION

In this section, we test the proposed UWB-based indoor human localization system operating with time-delay data and using the EFIR filter and the EKF as main estimators. The investigations were provided in the Machine Building of the University of Jinan, Jinan, China. The trade-off between the EKF-based Algorithm 1 and the EFIR-based Algorithm 2 is also investigated. Because the exact knowledge about noise is unavailable in our experiment, we will consider two groups of possible noise statistics.

A. PREPARATION STAGE

1) TEST ENVIRONMENT

To test the proposed human localization system and the proposed data fusion method, the indoor environment was created as shown in Fig. 2. In our test, four UWB RNs, one UWB BN, a computer, and a reference system were organized to interact on the indoor floorspace. Firstly, we fixed four UWB RNs at known coordinates. The UWB BN, a computer, and a reference system were placed on a human. Secondly, we have planed a reference path and then ordered a human to travel along it.

Fig.3 displays the testbed architecture used in this work. From the figure, we can see that the testbed used in this work includes three parts: the UWB RNs; one person with one UWB BN and the computer; and a reference system. In this work, we employ the DW1000-based UWB positioning system. To organize the UWB RNs, we employ four UWB RNs in the test (ID from #1 to #4). In Fig.3, we give a detailed structure of only one UWB RN node, which includes a UWB sender, a timer, a control processing module, and a power supply module.

A person equipped with one UWB BN and a computer is an important part of the testbed. Here, the UWB BN measures distances from the RNs to BN and all information collected in such a way is submitted to a computer. In order to provide a reference value, the person carry a reference system, which includes one encode to measure the distance from the start point. In this experiment, the sampling time for the UWB signal was chosen to be 0.3 s. Figure 4 displays the human equipment used to test the localization system. Provided the reference trajectory, we next test the human localization performance using two types of estimators: EKF and EFIR.

2) TUNING EFIR FILTER

It follows that Algorithm 2 requires only the size M of the state vector and the averaging horizon length N to start computing and updating the estimates using $\mathbf{y}_k^{td}$. In the state-space model (3) and (4), we have $M = 8$ and $\mathbf{y}_k^{td}$ is provided by the UWB-based measurements. To specify N optimally for the reference trajectory, the best way is to consider the estimation error covariance

$$\mathbf{P}_k^{td} = E\{(\mathbf{x}_k^{td} - \hat{\mathbf{x}}_k^{td})(\mathbf{x}_k^{td} - \hat{\mathbf{x}}_k^{td})^T\}, \tag{6}$$

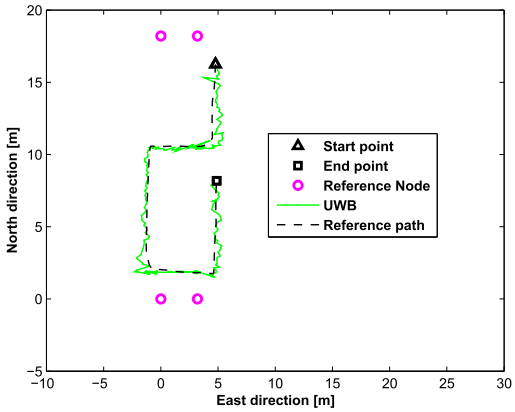

FIGURE 5. The reference planned path and trajectory derived from UWB.

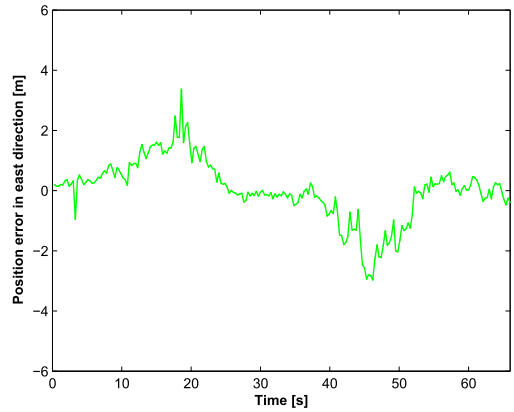

FIGURE 6. The east localization errors produced by the UWB.

TABLE 1. Absolute average localization errors, in m, produced by the INS and UWB.

Model	East direction		North direction	
	Mean	Stdev	Mean	Stdev
UWB	0.72	0.71	0.19	0.18

where $\mathbf{x}_k^{td}$ is the reference planned path, refer to [34], and estimate N_{opt} by solving the following optimization problem,

$$N_{\text{opt}} = \arg\min_N \{\text{tr}\, \mathbf{P}_k^{td}(N)\}. \tag{7}$$

Referring to the state-space model (3) and (4), the trace of $\mathbf{P}_k^{td}$ becomes

$$\text{tr}\, \mathbf{P}_k^{td}(N) = P_{55k}^{td}(N) + P_{77k}^{td}(N). \tag{8}$$

Note that it needs using all $\mathbf{x}_k^{td}$ to find N_{opt} via (7) and (8) that faces practical issues, especially in real time system. Thus, we set $N = M + 1 = 9$ as N_{opt} in this work.

3) SYSTEM CHARACTERISTICS

Figure 5 displays the reference trajectory used in this work and the trajectory derived from UWB. In this test, the UWB RNs (denote as pink circle) are fixed on the known coordinations. Then, the person walked along the reference path (denote as dotted line) from the start point (denote as triangle) to end point (denote as square). The trajectory derived from UWB is denoted by a green line.

As can be seen, the UWB is able to provide the human position. However, the UWB solution is noisy. More details about errors in the east and north directions is listed in Fig. 6 and Fig. 7, respectively. The absolute average localization error produced by the UWB is shown in Tab. 1. Note that the UWB position errors in the east and north directions are at levels of 0.72 m and 0.19 m, respectively. The east position error is bigger than that value in north direction.

In order to verify the performance of the proposed method, we select two groups of feasible parameters:

Group 1: $\mathbf{x}_0^{td} = \left[4.78\ 0\ 16.25\ 0\ 4.78\ 0\ 16.25\ 0\right]^T$, $\mathbf{Q}^{td} = \text{diag}\{0.1\ 0.01\ 0.1\ 0.01\ 0.1\ 0.01\ 0.1\ 0.01\}$, and $\mathbf{R}^{td} = \mathbf{I}_{4\times4}$, $\mathbf{P}_0^{td} = \mathbf{I}_{8\times8}$.

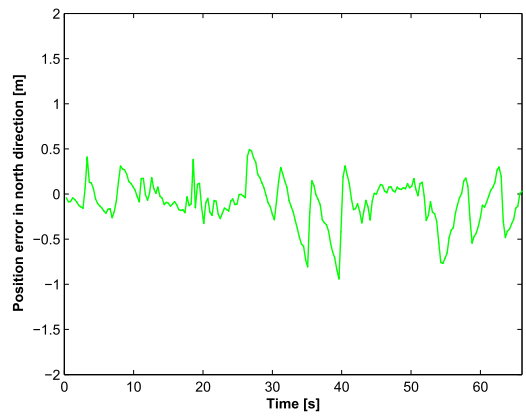

FIGURE 7. The north localization errors produced by the UWB.

Group 2: $\mathbf{x}_0^{td} = \left[4.78\ 0\ 16.25\ 0\ 4.78\ 0\ 16.25\ 0\right]^T$, $\mathbf{Q}^{td} = 10^{-5}\text{diag}\{0.1\ 0.01\ 0.1\ 0.01\ 0.1\ 0.01\ 0.1\ 0.01\}$, $\mathbf{P}_0^{td} = \mathbf{I}_{8\times8}$, and $\mathbf{R}^{td} = \mathbf{I}_{4\times4}$.

Because the coordinates of the start point are known, we set the initial vector as $\mathbf{x}_0^{td} = \left[4.78\ 0\ 16.25\ 0\ 4.78\ 0\ 16.25\ 0\right]^T$, where (4.78, 16.25) is the exact position of start point. Then, we set the initial error covariance matrix to be identity, $\mathbf{P}_0 = \mathbf{I}$. Because exact information about noise covariances $\mathbf{Q}$ and $\mathbf{R}$ is commonly unavailable in human localization, we suppose that both these matrices are identities with weights separated into Group 1 and Group 2. The EFIR filter produces the first estimate at $k = N_{\text{opt}} - 1$ and the last one at $k = SampleNumb$, where $SampleNumb$ is the number of the sample points.

B. LOCALIZATION ERRORS – GROUP 1

In the first experiment, we investigate the performance obtained for the Group 1 by 1) the UWB model using the least squares (LS) algorithm and 2) the UWB-based time-delay model employing the EKF and EFIR estimators. Figure 8 shows the trajectories measured by the UWB model using the LS algorithm and by the time-delay model employing the EKF and EFIR estimators for the Group 1 of parameters. From the figure, we can see that the Group 1 of the parameters

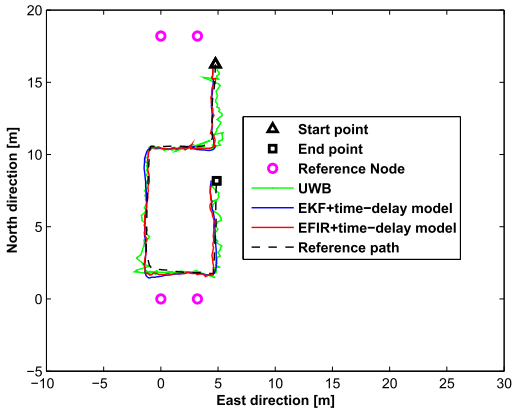

FIGURE 8. The trajectories measured by the UWB model using the LS algorithm and by the time-delay model employing the EKF and EFIR estimators for the Group 1 of parameters.

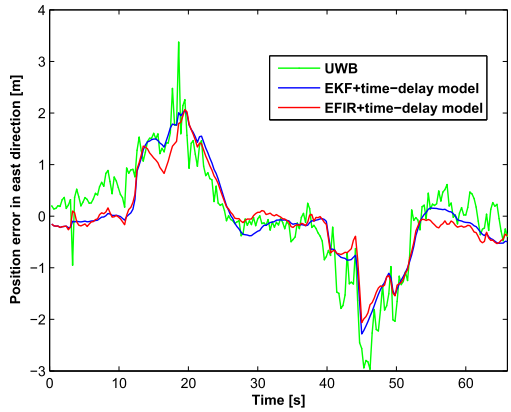

FIGURE 9. The east localization errors produced by the UWB model using the LS algorithm and by the time-delay model employing the EKF and EFIR estimators for the Group 1 of parameters.

fits the experiment and all the estimators provide the accurate human position well consistent with the reference path.

More details about errors in the east and north directions can be found in Fig. 9 and Fig. 10. From these figures, one can see that the UWB-based localization error in the east direction is bigger than that in the north direction. In the east direction, the UWB-based error ranges from -3 m to about 3 m. It is also seen that the error function in the north direction is more stable than in the east direction: it ranges from about -1 m to 1 m. Compared with the UWB solution, both the EKF and EFIR filter are able to reduce the localization errors and, for this group of parameters, errors by the EKF and EFIR estimators are closely related.

The absolute average localization errors produced by the EKF and EFIR estimators (Group 1) are listed in Table 2. It follows from this table that errors produced by both the EKF and EFIR filter are smaller than in the UWB solution. It can also be seen that the EFIR filter is more accurate in the east direction with the error of about 0.54 m. Of importance is that the EFIR estimator provides a very good performance with no requirements for the noise statistics.

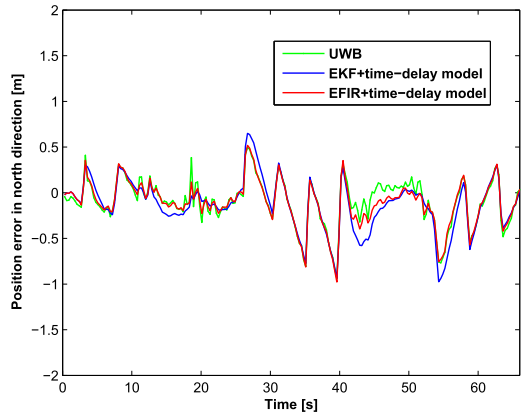

FIGURE 10. The north localization errors produced by the UWB model using the LS algorithm and by the time-delay model employing the EKF and EFIR estimators for the Group 1 of parameters.

TABLE 2. Absolute average localization errors, in m, produced by the EKF and EFIR estimators (Group 1).

Model	East direction		North direction	
	Mean (m)	Stdev (m)	Mean (m)	Stdev (m)
UWB	0.72	0.71	0.19	0.18
EKF	0.58	0.62	0.21	0.19
EFIR	0.54	0.57	0.19	0.18

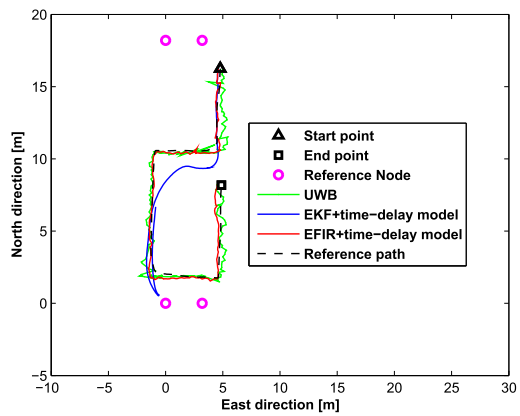

FIGURE 11. The trajectory measured by the UWB model using the LS algorithm and by the time-delay model employing the EKF and EFIR estimators for the Group 2 of parameters.

C. LOCALIZATION ERRORS – GROUP 2

In the second experiment, we provide the localization for the Group 2 of parameters. Here, we set the system noise covariance matrix $\mathbf{Q}^{td}$ to be gained by the factor of 10^{-5}. Figure 11 shows the trajectories measured by the UWB model using the LS algorithm and estimated employing the EKF and EFIR filter. This figure reveals that the EKF diverges and its estimates becomes unacceptable. Based upon this observation, we deduce that the Group 2 of parameters does not fit the experiment. Just on the contrary, the EFIR filter allows for the human localization with acceptable errors. That means that the EFIR filter has much higher robustness that the EKF.

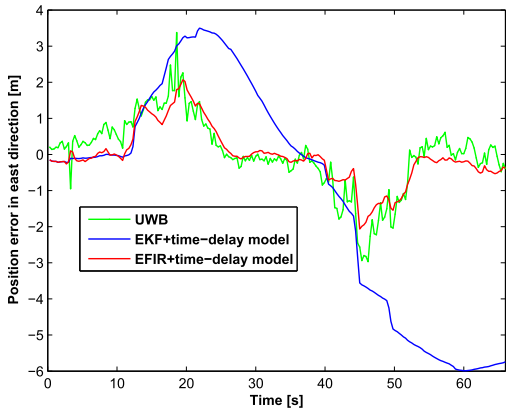

FIGURE 12. The east localization errors produced by the UWB model using the LS algorithm and by the time-delay model employing the EKF and EFIR estimators for the Group 2 of parameters.

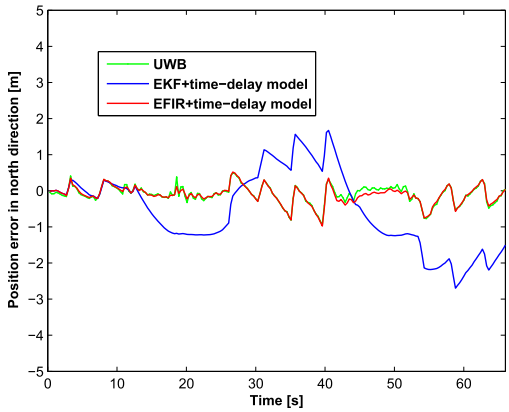

FIGURE 13. The north localization errors produced by the UWB model using the LS algorithm and by the time-delay model employing the EKF and EFIR estimators for the Group 1 of parameters.

TABLE 3. Absolute average localization errors, in m, produced by the EKF and EFIR estimators (Group 2).

Model	East direction		North direction	
	Mean (m)	Stdev (m)	Mean (m)	Stdev (m)
UWB	0.72	0.71	0.19	0.18
EKF	2.79	2.39	1.55	1.86
EFIR	0.54	0.57	0.19	0.18

The localization errors produced by the UWB, EKF, and EFIR filter in the east and north directions are shown in Fig. 12 and Fig. 13, respectively. It follows from Fig. 12 and Fig. 13 that the EKF becomes biased when the predicted $\mathbf{Q}^{td}$ reduces. On the contrary, the EFIR estimator does not demonstrate any deviation, because this filter ignores $\mathbf{Q}^{td}$ in the algorithm. The averaged absolute localization errors produced by the EKF and EFIR estimators (Fig. 12 and Fig. 13) are listed in Table 3. This table suggests that the EKF performance is poor for the Group 2 of parameters, while the EFIR filter performance is quite appropriate for the localization.

V. CONCLUSION

In this work, the UWB technology is applied to provide indoor human localization. Because time delays often accompany the measurements, we have developed the UWB-based time-delay human localization scheme with an augmented state vector supposing that data arrive at an estimator with or without the one-step delay. The EKF and EFIR filter were exploited as main estimators. The experimental investigations have shown that when the noise statistics are known more or less accurately (that may not be the case in many applications), then both estimators produce similar errors consistent to the UWB solution. Otherwise, the EKF may diverge and its performance become very poor. On the contrary, no such effects were observed at the EFIR filter output. An overall conclusion is that the EFIR filter maybe a better choice that the EKF for indoor human localization under the real world operation conditions in not well specified noise environments.

REFERENCES

[1] Y. Sun, W. Meng, C. Li, N. Zhao, K. Zhao, and N. Zhang, "Human localization using multi-source heterogeneous data in indoor environments," *IEEE Access*, vol. 5, pp. 812–822, Jan. 2017.
[2] W. Li and Y. Jia, "Location of mobile station with maneuvers using an IMM-based cubature Kalman filter," *IEEE Trans. Ind. Electron.*, vol. 59, no. 11, pp. 4338–4348, Nov. 2012.
[3] Y. Xu and X. Chen, "Online cubature Kalman filter Rauch-Tung-Striebel smoothing for indoor inertial navigation system/ultrawideband integrated pedestrian navigation," *Proc. Inst. Mech. Eng. I, J. Syst. Control Eng.*, pp. 1–9, 2017.
[4] Z.-Q. Zhang and X. Meng, "Use of an inertial/magnetic sensor module for pedestrian tracking during normal walking," *IEEE Trans. Instrum. Meas.*, vol. 64, no. 3, pp. 776–783, Mar. 2015.
[5] A. Belakbir, M. Amghar, N. Sbiti, and A. Rechiche, "An indoor-outdoor positioning system based on the combination of GPS and UWB sensors," *J. Theor. Appl. Inf. Technol.*, vol. 61, no. 1, pp. 67–72, Mar. 2014.
[6] Q. Li, W. Li, W. Sun, and J. Li, "Fingerprint and assistant nodes based WiFi localization in complex indoor environment," *IEEE Access*, vol. 4, pp. 2993–3004, Jun. 2016.
[7] Y. Zhuang, Z. Syed, J. Georgy, and N. El-Sheimy, "Autonomous smartphone-based WiFi positioning system by using access points localization and crowdsourcing," *Pervasive Mobile Comput.*, vol. 18, pp. 118–136, Feb. 2015.
[8] B. Benjamin, G. Erinc, and S. Carpin, "Real-time WiFi localization of heterogeneous robot teams using an online random forest," *Auto. Robots*, vol. 39, no. 2, pp. 155–167, Aug. 2015.
[9] J. J. Pomárico-Franquiz, M. Granados-Cruz, and Y. S. Shmaliy, "Self-localization over RFID tag grid excess channels using extended filtering techniques," *IEEE J. Sel. Topics Signal Process.*, vol. 9, no. 2, pp. 229–238, Mar. 2015.
[10] Z. Zhang, Z. Lu, V. Saakian, X. Qin, Q. Chen, and L.-R. Zheng, "Item-level indoor localization with passive UHF RFID based on tag interaction analysis," *IEEE Trans. Ind. Electron.*, vol. 61, no. 4, pp. 2122–2135, Apr. 2013.
[11] X. Tan, M. Dong, C. Wu, K. Ota, J. Wang, and D. W. Engels, "An energy-efficient ECC processor of UHF RFID tag for banknote anti-counterfeiting," *IEEE Access*, vol. 5, pp. 3044–3054, 2016.
[12] Y. Xu, X. Chen, J. Cheng, Q. Zhao, and Y. Wang, "Improving tightly-coupled model for indoor pedestrian navigation using foot-mounted IMU and UWB measurements," in *Proc. IEEE Int. Instrum. Meas. Technol. Conf.*, May 2016, pp. 1–5.
[13] L. Zwirello, T. Schipper, M. Harter, and T. Zwick, "UWB localization system for indoor applications: Concept, realization and analysis," *J. Elect. Comput. Eng.*, vol. 2012, no. 5, p. 4, Mar. 2012.
[14] L. Zhu and X. Cheng, "High manoeuvre target tracking in coordinated turns," *IET Radar, Sonar Navigat.*, vol. 9, no. 8, pp. 1078–1087, Sep. 2015.
[15] K. Kobai, Y. Kosuge, and I. Matsunami, "Transient response performance of a decoupling filter with variable sampling intervals using a constant acceleration model," *Tech. Rep. IEICE Sane*, vol. 112, no. 10, pp. 13–17, Oct. 2013.
[16] R. A. Singer, "Estimating optimal tracking filter performance for manned maneuvering targets," *IEEE Trans. Aerosp. Electron. Syst.*, vol. AES-6, no. 4, pp. 473–483, Jul. 1970.

[17] Z. Feng and J. Lam, "On reachable set estimation of singular systems," *Automatica*, vol. 52, pp. 146–153, Feb. 2015.
[18] Z. Feng and W. X. Zheng, "Improved stability condition for Takagi–Sugeno fuzzy systems with time-varying delay," *IEEE Trans. Cybern.*, vol. 47, no. 3, pp. 661–670, Mar. 2017.
[19] Z. Feng, W. Li, and J. Lam, "Dissipativity analysis for discrete singular systems with time-varying delay," *ISA Trans.*, vol. 64, pp. 86–91, Sep. 2016.
[20] Z.-G. Wu, P. Shi, H. Su, and J. Chu, "Dissipativity analysis for discrete-time stochastic neural networks with time-varying delays," *IEEE Trans. Neural Netw. Learn. Syst.*, vol. 24, no. 3, pp. 345–355, Mar. 2013.
[21] Z. Feng, J. Lam, and G.-H. Yang, "Optimal partitioning method for stability analysis of continuous/discrete delay systems," *Int. J. Robust Nonlinear Control*, vol. 25, no. 4, pp. 559–574, Mar. 2015.
[22] Q. Zhou, D. Yao, J. Wang, and C. Wu, "Robust control of uncertain semi-Markovian jump systems using sliding mode control method," *Appl. Math. Comput.*, vol. 286, pp. 72–87, Aug. 2016.
[23] L. Wang, H. Li, Q. Zhou, and R. Lu, "Adaptive fuzzy control for nonstrict feedback systems with unmodeled dynamics and fuzzy dead zone via output feedback," *IEEE Trans. Cybern.*, vol. 47, no. 9, pp. 2400–2412, Apr. 2017.
[24] B. Chen, W. Zhang, G. Hu, and L. Yu, "Networked fusion Kalman filtering with multiple uncertainties," *IEEE Trans. Aerosp. Electron. Syst.*, vol. 51, no. 3, pp. 2232–2249, Jul. 2015.
[25] M. Van, S. S. Ge, and H. Ren, "Finite time fault tolerant control for robot manipulators using time delay estimation and continuous nonsingular fast terminal sliding mode control," *IEEE Trans. Cybern.*, vol. 47, no. 7, pp. 1681–1693, Jul. 2016.
[26] B. Chen, W.-A. Zhang, and L. Yu, "Distributed fusion estimation with missing measurements, random transmission delays and packet dropouts," *IEEE Trans. Autom. Control*, vol. 59, no. 7, pp. 1961–1967, Jul. 2014.
[27] L. Zhao, H. Qiu, and Y. Feng, "Analysis of a robust Kalman filter in loosely coupled GPS/INS navigation system," *Measurement*, vol. 80, no. 12, pp. 138–147, Dec. 2016.
[28] J. Fang and X. Gong, "Predictive iterated Kalman filter for INS/GPS integration and its application to SAR motion compensation," *IEEE Trans. Instrum. Meas.*, vol. 59, no. 4, pp. 909–915, Apr. 2010.
[29] M. Narasimhappa, J. Nayak, M. H. Terra, and S. L. Sabat, "ARMA model based adaptive unscented fading Kalman filter for reducing drift of fiber optic gyroscope," *Sens. Actuators A, Phys.*, vol. 251, pp. 42–51, Nov. 2016.
[30] Y. Zhao, "Cubature + extended hybrid Kalman filtering method and its application in PPP/IMU tightly coupled navigation systems," *IEEE Sensors J.*, vol. 15, no. 12, pp. 6973–6985, Dec. 2015.
[31] I. C. Schick and S. K. Mitter, "Robust recursive estimation in the presence of heavy-tailed observation noise," *Ann. Statist.*, vol. 22, no. 2, pp. 1045–1080, Jun. 1994.
[32] Y. S. Shmaliy and D. Simon, "Iterative unbiased FIR state estimation: A review of algorithms," *EURASIP J. Adv. Signal Process.*, vol. 2013, no. 1, p. 113, Jan. 2013.
[33] Y. S. Shmaliy, "Suboptimal FIR filtering of nonlinear models in additive white Gaussian noise," *IEEE Trans. Signal Process.*, vol. 60, no. 10, pp. 5519–5527, Oct. 2012.
[34] F. Ramirez-Echeverria, A. Sarr, and Y. S. Shmaliy, "Optimal memory for discrete-time FIR filters in state-space," *IEEE Trans. Signal Process.*, vol. 62, no. 3, pp. 557–561, Feb. 2014.

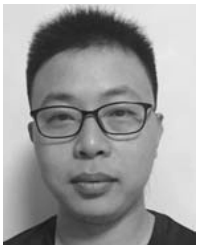

YUAN XU (M'16) received the B.S. degree in automation from Shandong Polytechnic University in 2007, the M.S. degree in detection technology and automation device from Shandong Polytechnic University in 2010, and the Ph.D. degree in instrument science from Southeast University in 2014. He is currently a Lecturer with the School of Electrical Engineering, University of Jinan, Jinan, China. His research interests include integrated navigation and robust filtering.

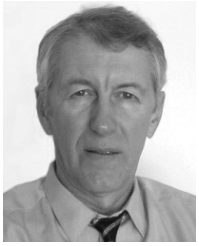

YURIY S. SHMALIY (M'96–SM'00–F'11) received the B.S., M.S., and Ph.D. degrees in electrical engineering from the Kharkiv Aviation Institute, Kharkiv, Ukraine, in 1974, 1976, and 1982, respectively, and the D.Sc. degree from the Kharkiv Railroad Institute, Kharkiv, in 1992. He has been a Full Professor since 1986. From 1985 to 1999, he was with Kharkiv Military University, Kharkiv, Ukraine. In 1992, he founded the Scientific Center, Sichron, where he became the Director by 2002. Since 1999, he has been with the Universidad de Guanajuato, Leon, Mexico, where he headed the Department of Electronics Engineering from 2012 to 2015. From 2015 to 2016, he has been a Visiting Professor with City, University of London, London, U.K., and in 2015 and 2017, a Visiting Researcher with the TELECOM SudParis.

He has 381 journal and conference papers and 81 patents. His has authored the books entitled *Continuous-Time Signals* (Springer, 2006), *Continuous-Time Systems* (Springer, 2007), and *GPS-Based Optimal FIR Filtering of Clock Models* (Nova Science Publication, New York, 2009). He also edited a book *Probability: Interpretation, Theory and Applications* (Nova Science Publication, New York, 2012) and contributed to several books with invited chapters. He was invited many times to give tutorial, seminar, and plenary lectures. His current interests include optimal estimation, statistical signal processing, and stochastic system theory. He was awarded a title, Honorary Radio Engineer of the USSR, in 1991. He was listed in Outstanding People of the 20th Century, Cambridge, U.K., in 1999 and received the Royal Academy of Engineering Newton Research Collaboration Program Award in 2015. He is currently an Associate Editor and an Editorial Board Member in several journals.

YUEYANG LI (M'17) received the B.Sc. and Ph.D. degrees in control theory and control engineering from Shandong University, China, in 2006 and 2011, respectively. In 2014, he was a Visiting Scholar with the SUCRO Laboratory, Shandong University. In 2015, he was a Visiting Scholar with the Institute for Automatic Control and Complex Systems, University of Duisburg–Essen, Germany. He is currently an Associate Professor with the School of Electrical Engineering, University of Jinan, Jinan, China. His main research interests include fault detection for time-varying systems and robust filtering for stochastic systems.

XIYUAN CHEN (M'08–SM'13) received the B.S. degree in mechanical engineering from the Lanzhou University of Technology, China, in 1990, the M.Sc. degree in mechanical engineering from the Hefei University of Technology, China, in 1995, and the Ph.D. degree in precision instrument and mechanical engineering from Southeast University, China, in 1998. He is currently a Professor with the School of Instrument Science and Engineering, Southeast University. His research interests include inertial navigation and integrated measurement.